A fiducial detection algorithm for real-time image guided IMRT based on simultaneous MV and kV imaging

Weihua Mao, Nadeem Riaz, Louis Lee, Rodney Wiersma, and Lei Xing[a)]
Department of Radiation Oncology, Stanford University School of Medicine, Stanford, California 94305-5847

(Received 9 January 2008; revised 2 May 2008; accepted for publication 11 June 2008; published 11 July 2008)

The advantage of highly conformal dose techniques such as 3DCRT and IMRT is limited by intrafraction organ motion. A new approach to gain near real-time 3D positions of internally implanted fiducial markers is to analyze simultaneous onboard kV beam and treatment MV beam images (from fluoroscopic or electronic portal image devices). Before we can use this real-time image guidance for clinical 3DCRT and IMRT treatments, four outstanding issues need to be addressed. (1) How will fiducial motion blur the image and hinder tracking fiducials? kV and MV images are acquired while the tumor is moving at various speeds. We find that a fiducial can be successfully detected at a maximum linear speed of 1.6 cm/s. (2) How does MV beam scattering affect kV imaging? We investigate this by varying MV field size and kV source to imager distance, and find that common treatment MV beams do not hinder fiducial detection in simultaneous kV images. (3) How can one detect fiducials on images from 3DCRT and IMRT treatment beams when the MV fields are modified by a multileaf collimator (MLC)? The presented analysis is capable of segmenting a MV field from the blocking MLC and detecting visible fiducials. This enables the calculation of nearly real-time 3D positions of markers during a real treatment. (4) Is the analysis fast enough to track fiducials in nearly real time? Multiple methods are adopted to predict marker positions and reduce search regions. The average detection time per frame for three markers in a 1024×768 image was reduced to 0.1 s or less. Solving these four issues paves the way to tracking moving fiducial markers throughout a 3DCRT or IMRT treatment. Altogether, these four studies demonstrate that our algorithm can track fiducials in real time, on degraded kV images (MV scatter), in rapidly moving tumors (fiducial blurring), and even provide useful information in the case when some fiducials are blocked from view by the MLC. This technique can provide a gating signal or be used for intra-fractional tumor tracking on a Linac equipped with a kV imaging system. Any motion exceeding a preset threshold can warn the therapist to suspend a treatment session and reposition the patient.
[DOI: 10.1118/1.2953563]

I. INTRODUCTION

Highly conformal radiation therapy techniques, such as three-dimensional conformal radiotherapy (3DCRT) and intensity-modulated radiation therapy[1] (IMRT), provide exquisitely shaped radiation doses that closely conform to tumor dimensions while sparing sensitive structures.[1,2] They require greater precision in tumor localization, treatment setup, and delivery than conventional techniques. In practice, inter- and intrafraction organ motion results in an uncertainty of tumor location. For example, respiratory and prostate tumors can move up to 3 cm over the course of routine radiotherapy.[3–9] Research activities on image-guided radiation therapy have emerged recently to improve targeting in radiation treatment.[10] It is essential to track the dynamical nature of human anatomy or at least the tumor motion in real time.[11]

Several methods of obtaining the real-time tumor position are available, and these can be categorized as being either indirect (external surrogate based) or direct (fiducial/image) in nature. In general, indirect tumor location methods, such as external skin marker tracking or breath monitoring techniques, rely on the correlation between external body parameters and the tumor.[5,12] In reality, the relationship between external parameters and internal organ motion is complex and a large uncertainty may be present in predicting the tumor location based on external markers. Direct tumor position measurement is highly desirable for therapeutic guidance. In the last decade, a number of direct real-time 3D tumor tracking methods have been implemented, primarily using fluoroscopy[5,11,13] or magnetic field localization.[14] Particularly, the feasibility of using electronic portal imaging devices (EPID) and stereoscopic x-ray imaging for real-time tumor tracking has been explored.[3,5,6,15–26]

A crucial component of an image based tracking system is the ability to successfully identify and track user-specified image-based features at a near real-time speed. The detection algorithm must also be able to segment markers from anatomic structures and simultaneously track multiple markers without confusing one marker for another. Generally, an intensity based fiducial marker detection algorithm tends to fail when the marker is in the vicinity of high contrast structures such as bone. This can be avoided by using template matching, as demonstrated by Shirato *et al.*, for the tracking of a single spherical gold marker using multiple kV fluoroscopic

imaging systems.[25] Tang *et al.* have further extended template matching by developing a cylindrical marker detection algorithm that takes into account the different possible projections of the marker based on its orientation and length on their custom designed stereoscopic kV on-board imaging systems.[27] Because a single in-line x-ray beam is only two dimensional, the 3D coordinates of the embedded fiducials are usually obtained by specially designed multiple kV x-ray sets.[3,5,6,25–28]

Recently, Wiersma *et al.* used combined kV and MV imaging systems to track the 3D location of a spherical metallic fiducial.[29] This technique has the inherent benefit in that only one kV source is required for full 3D marker positional information since the actual MV beam is also used for positioning. Compared to other stereoscopic systems, which generally require two or more kV imaging sets, this technique reduces the radiation dose to the patient and requires minimal modification of the current hardware. In Wiersma's work, a freely available third party software program was used to detect a spherical fiducial, 3 mm in diameter. As of yet, there have been few works presenting marker-tracking algorithms that are suitable for tracking internal markers using MV image data with high success rates because these images have significantly reduced contrast.[18] Further, it is a more challenging task to robustly detect small cylindrical fiducials (gold seeds) used clinically, in a realistic setting. This problem is exacerbated when the incident beam is an IMRT field instead of an open field, because one or all implanted fiducials may be blocked by the MLC at some segments during IMRT delivery.

In this article, using a new detection algorithm,[30] we will study four clinically relevant issues pertaining to the application of tracking fiducials in real time based on simultaneous kV and MV imaging:

(1) How fast can a marker move and still be detectable? Motion will blur the fiducial and hinder tracking it. It is essential to investigate the maximum moving speed at which the markers can still be detected by this procedure.
(2) How does the MV beam scattering affect kV imaging? It has been reported that if MV and kV images are acquired simultaneously, MV beam scattering has significant interference with kV imaging while kV beam scattering effect on MV images is minor.[31] A quantitative study is necessary to clarify if simultaneous MV beam scattering affects the detection of markers on kV images.
(3) Can an algorithm reliably track markers in MV images with irregular fields? The aperture of MV beam is carefully modified by a multiple-leaf collimator (MLC) in any 3DCRT or IMRT treatment plans. A major challenge is that one or more markers may be outside of the MV fields/ images and this requires very high specificity detection, particularly when the MLC is moving. Is this tracking procedure capable of handling the MLC blocking problem?
(4) Is this algorithm fast enough to track markers in nearly real time? An analysis speed of 10 Hz is desirable for a nearly real-time 3D position tracking in order to gate treatment beam delivery.

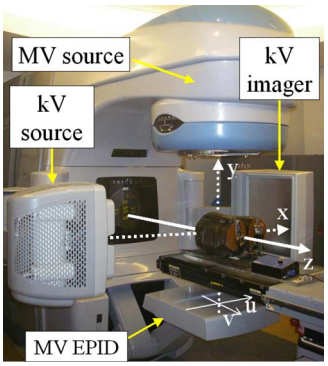

FIG. 1. A picture of the Trilogy with extended MV EPID, kV source, and kV imager. Room coordinates are illustrated.

II. MATERIALS AND METHOD

II.A. Hardware setup and computer calculation

All experiments were performed on a Varian Trilogy™ (Varian Medical System, Palo Alto, CA) with a MV EPID and a kV onboard imaging system as shown in Fig. 1. The onboard imaging system is located perpendicular to the treatment MV beam and consists of a kV x-ray tube together with an *a*Si flat panel imager. Effective pixel sizes of the kV and MV detectors were 0.388 and 0.392 mm, respectively. Both detectors had a resolution of 1024×768, corresponding to an effective area of detection of approximately 40 cm $\times$ 30 cm. For both MV and kV systems, the default source-to-axis distances (SADs) and source-to-imager distances (SIDs) were set to 100 and 150 cm, respectively. Both dual MV energies, 6 and 15 MV, were used in this article. The MV EPID was capable of capturing images at a speed of 7.5 frames per second (fps) and 7.8 fps for 6 and 15 MV beams, respectively, while the kV imager had a capturing speed of 15 fps in the fluoroscopic or continuous imaging mode.

A sliced pelvic phantom was tested on a motion platform. Three gold cylindrical fiducial markers were embedded in the prostate position, each fiducial had a diameter of 1.2 mm and a length of 3.0 mm. The platform was driven by an electrical motor and could move linearly with an adjustable period between 2.0 and 6.0 s and its maximum motion amplitude was set to 1.0 cm.

A software program (C language) was developed to analyze projection images and obtain fiducial positions. All calculations were performed on a Dell Precision 470 workstation (3.4 GHz Xeon CPU and 4 GB RAM).

II.B. Fiducial tracking algorithm

Figure 2 illustrates the complete procedure to track markers on open-field kV or MV images. Major steps are described in the following subsections.

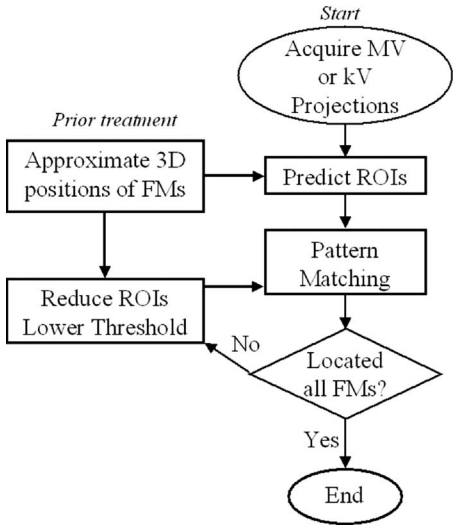

FIG. 2. Flow chart of detecting moving markers on open-field kV/MV images.

- Obtain approximate 3D positions of FMs from planning CT

  The first step was to obtain approximate 3D positions of fiducials from the planning CT and then convert them to the treatment coordinates. A simple intensity-based search for the markers was performed on the planning CT. Due to the much larger CT numbers of the metallic markers relative to other anatomical structures, the markers were easily segmented from the image background. The displacement vector relating the CT iso-center to the treatment iso-center was then used to relocate marker CT coordinates relative to the treatment iso-center.
- Predict FM locations

  The FM locations on projection images could be predicted by their approximate 3D positions obtained from prior planning CT images. For any FM having 3D position (x_M, y_M, z_M), its expected projection location (u, v) on either the kV or MV detector was predicted by the following relationships:[32]

$$u = F\frac{\cos(\phi)x_M + \sin(\phi)y_M}{R - \sin(\phi)x_M + \cos(\phi)y_M} \quad (1)$$

$$v = F\frac{z_M}{R - \sin(\phi)x_M + \cos(\phi)y_M}, \quad (2)$$

  where ϕ was the Varian gantry angle, R was SAD, and F was SID. The x axis was in the lateral direction of patient couch, the y axis was in the anterior-posterior[7] direction, the z axis was the superior-interior (SI) direction, and the origin was the Linac's iso-center. The coordinates of the imagers (u, v) were defined on the imager and rotated with the gantry while v axis was parallel to z axis and u-axis laying the xy plane. Their origin is at the imager geometric center and their units are in mm or pixels (converted by effective pixel size).

  The region to search for the fiducial marker was then reduced to a small circular region of interest (ROI) centered on the predicted location. The ROI may be large or small depending on the range of tumor motion. Typically, a ROI with a radius of 75 pixels, or about 2 cm around the object, was found to be adequate for locating the moving markers in our studies.

  For those markers located near each other, overlapping ROIs were combined into one larger ROI group containing both markers. In the case of multiple markers existing in the same ROI group, the detected marker positions in this ROI group were reordered based on the information from the planning CT results including the internal distances between markers and the shortest distances between detected and predicted marker projections, so that every detected fiducial would be identified without any confusion.
- Reduce ROIs

  Two methods were used to reduce ROIs if possible. One method was to use the detected FM locations on the previous image during a continuous imaging course. Due to the short time interval between acquisitions (<0.1 s) marker movement between consecutive images was limited so the new FM location should be close to the prior location. For instance, when the ROI radius was reduced to 25 pixels, this still covered a region with a radius of 6.7 mm, which corresponded to any movement with a speed less than 5 cm/s.

  Another method was to use the relative positions among markers to locate undetected markers under the rigid body assumption. As long as one or more markers were detected, other markers' expected positions were calculated based on their relative locations to the detected markers by ignoring the internal motion among markers. The second search was usually performed in smaller ROIs with lower thresholds in order to detect markers with a weaker signal.
- Match patterns

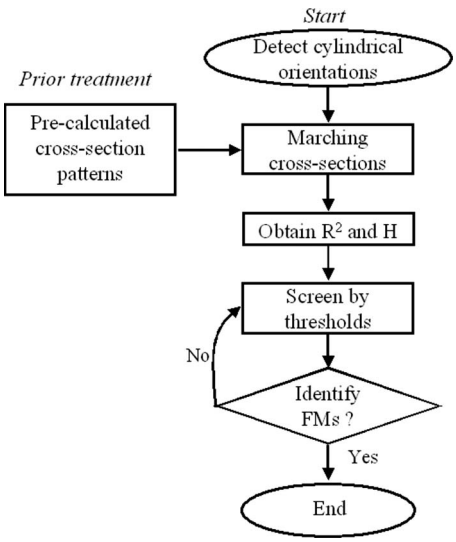

FIG. 3. Flow chart of pattern matching algorithm.

A novel fiducial tracking algorithm (pattern matching algorithm, as summarized in Fig. 3) has been developed to detect cylindrical fiducial markers on kV and MV projection images.[20,30] A cylindrical marker could be projected into different shapes depending on its orientation. A filter was applied to find the fiducial orientation at a given pixel. With this filter, we divided the angular space on a projection plane into eight bins. The average intensities of every bin adjacent to the given pixel were compared and the bin with the highest average intensity was presumed to correspond to the fiducial orientation. It should be noted that the cylindrical orientation results carried no information for most of the pixels and it was only valid for pixels on a cylindrical object.

A cylindrical marker can be projected into different shapes (length and orientation) depending on its orientation and the x-ray beam direction. However, its cross section, a narrow section perpendicular to the cylindrical orientation, is a unique feature and it only depends on the fiducial width and cylindrical orientation. For convenience, the cross-section patterns at all eight cylindrical orientations were precalculated for given widths. The cross section of every pixel was then matched with the predetermined cross-section pattern at the cylindrical orientation of that center pixel. At each pixel location (u,v) within ROIs, a comparison was made between the surrounding pixels ($\{f_{u+i,v+j}\}$) and the pattern ($\{p_{i,j}\}$) corresponding to the cylindrical orientation of that pixel. Two criteria were used to quantify the matching: The square of the correlation coefficient, $R^2_{u,v}$, and the scaling factor or intensity, $H_{u,v}$,

$$R^2_{u,v}=\frac{\Sigma_{(i,j)\in\text{Pattern}}(f_{u+i,v+j}-\overline{f_{u,v}})(p_{i,j}-\bar{p})}{\sqrt{\Sigma_{(i,j)\in\text{Pattern}}(f_{u+i,v+j}-\overline{f_{u,v}})^2}\cdot\sqrt{\Sigma_{(i,j)\in\text{Pattern}}(p_{i,j}-\bar{p})^2}}, \tag{3}$$

$$H_{u,v}=\frac{\Sigma_{(i,j)\in\text{Pattern}}(f_{u+i,v+j}-\overline{f_{u,v}})(p_{i,j}-\bar{p})}{\Sigma_{(i,j)\in\text{Pattern}}(p_{i,j}-\bar{p})^2}, \tag{4}$$

where $\overline{f_{u,v}}$ is the average intensity of the pattern region around pixel (u,v) and $\bar{p}$ is the average intensity of the pattern distribution as given by

$$\overline{f_{u,v}}=\frac{1}{N}\sum_{(i,j)\in\text{Pattern}}f_{u+i,v+j}, \tag{5}$$

$$\bar{p}=\frac{1}{N}\sum_{(i,j)\in\text{Pattern}}p_{i,j}, \tag{6}$$

with N being the total pixel number of the pattern. The square of the coefficient of correlation or coefficient of determination for a linear regression is conveniently called R square or R^2. It varied from 0 (no correlation) to 1 (perfect correlation). The scaling factor, H, indicated the relative intensity of the object compared to the background. In an ideal case, the image was scaled from the pattern after a background shift, $f_{u+i,v+j}=k\cdot p_{i,j}+b$, where k and b were constants, and the pattern matching result would be $R^2_{u,v}=1$ and $H_{u,v}=k$.

After the R^2 and H values were calculated for every pixel in the ROIs, they were screened based on predefined thresholds. For pixels that passed the threshold, adjacent pixels were examined, and an overall length for the fiducial was determined. The presumed fiducial would be rejected if its overall length was longer than a predefined maximum length.

- **Calculate 3D coordinates from orthogonal dual projections**

The nearly real-time 3D positions of fiducial markers were calculated from FM projections on two orthogonal imagers. Every marker (x_M,y_M,z_M) had two projections: $(u_{\text{MV}},v_{\text{MV}})$ on MV imager and $(u_{\text{kV}},v_{\text{kV}})$ on kV imager. The Trilogy might have a different SID and SAD, $(F_{\text{MV}},R_{\text{MV}})$ and $(F_{\text{kV}},R_{\text{kV}})$, for the MV and kV imaging systems. Because the Trilogy kV imaging system always had a gantry angle of 90° larger than the MV imaging system, it is convenient to use the MV gantry angle to represent the Trilogy's rotation status. At a MV gantry angle of ϕ, the fiducial marker's coordinates could be calculated from Eqs. (1) and (2):

$$\alpha=u_{\text{MV}}\frac{F_{\text{kV}}R_{\text{MV}}+R_{\text{kV}}u_{\text{kV}}}{F_{\text{MV}}F_{\text{kV}}+u_{\text{MV}}u_{\text{kV}}}, \tag{7}$$

$$\beta=u_{\text{kV}}\frac{F_{\text{MV}}R_{\text{kV}}-R_{\text{MV}}u_{\text{MV}}}{F_{\text{MV}}F_{\text{kV}}+u_{\text{MV}}u_{\text{kV}}}, \tag{8}$$

$$x_{\text{FM}}=\cos(\phi)\cdot\alpha-\sin(\phi)\cdot\beta, \tag{9}$$

$$y_{\text{FM}}=\sin(\phi)\cdot\alpha+\cos(\phi)\cdot\beta, \tag{10}$$

$$z_{\text{FM}}=\frac{1}{2}\left(\frac{R_{\text{MV}}+\beta}{F_{\text{MV}}}v_{\text{MV}}+\frac{R_{\text{kV}}-\alpha}{F_{\text{kV}}}v_{\text{kV}}\right). \tag{11}$$

II.C. Experiments

- **Speed of moving FMs**

The motion of fiducials would blur images and impede tracking. The maximum detectable moving speed is an important factor of this detection procedure. We tracked fiducial markers implanted in a phantom, which moved at various speeds, on open-field kV and MV images. The maximum linear speed can be calculated by Eq. (12)

$$\text{speed} = \frac{2\pi A}{T}, \tag{12}$$

where A was the motion amplitude and it was 10.0 mm in this study and T was the motion period.

Detection efficiency has been defined as the ratio between total number of detected fiducials and total number of fiducials in all images.

- **Test the effects of MV scattering on kV imaging**

During simultaneous MV and kV imaging, scattering of the MV beam would significantly diminish kV imaging quality, but the diminished kV image might still be good enough to track fiducial markers. In general, the quality of kV images was inversely proportional to MV beam size and directly proportional to kV SID. In this study, the kV images were analyzed by varying the MV field size from the maximum of 26×20 cm^2 (open field) to 10×10 cm^2 and increasing the SID from 150.0 to 181.8 cm. Since the typical human abdomen has different thickness in lateral (LAT) and anterior-posterior directions and MV and kV beams are in orthogonal directions, the scattering effects on both AP and LAT directions were tested here.

- **Tracking fiducials with the presence of a MLC**

In order to track fiducials during a treatment course, two phantom verification plans for 3DCRT and IMRT treatments from real patients were prepared on an Eclipse (Varian Medical System, Palo Alto, CA). The 3DCRT plan contains four fields: AP, PA, and two LAT fields. The step and shoot IMRT treatment plan included seven fields and 74 segments in total. All MV and kV images were acquired simultaneously during the delivery of the treatment plans. The pelvic phantom was placed on the motion platform and both plans were delivered multiple times at different motion cycle periods.

Figure 4 shows the flow chart to track markers when the MLC was moving (i.e., for an IMRT plan). An identical tracking method was applied for kV images as described in Sec. II B. The kV results were then used to help locate fiducials on MV images as shown in Fig. 4. Compared to tracking markers on open-field images, there was an additional step to screen and define the MLC field after MV images were acquired. An intensity threshold was computed from the minimum and maximum intensity of the whole image and then used for segmenting the MV field from the MLC blocked area by a simple intensity based screening process. The image was also linearly normalized for consistent analysis across a series of projections. For convenience, the maximum intensity was normalized to 1000 while the minimum intensity was normalized to 0.

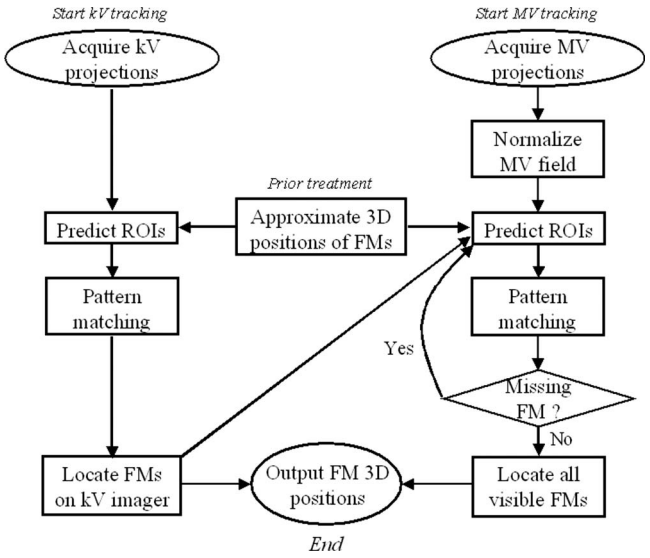

FIG. 4. Flow chart of detecting moving markers on IMRT kV/MV images.

When using the treatment MV beam for in-line imaging, a potential difficulty is that the fiducials may be partially or completely blocked by the MLC at certain segments. There are five sources of information can help in this situation. First, the coordinates of any fiducial from the orthogonal kV imaging are always available. This piece of information is very valuable in estimating the position of this fiducial on MV imager because the kV projection result indicates that the fiducial locates on a kV x-ray trace from the kV source to the kV projection. Its possible projection on MV imager must be on the projection of this kV x-ray trace. Coordinates of kV and MV projections of the same fiducial on the common axis, the v axis, are close to each other. More details are presented in the Appendix. Second, fiducial kinetics obtained at the previous time point can be utilized by a prediction algorithm to facilitate estimation of marker position as discussed in the subsection II B. **Fiducial tracking algorithm, Reduce ROIs**. Third, the detected fiducials' positions could be helpful to locate other blocked fiducials based on their relative positions as discussed in the subsection II B. **Fiducial tracking algorithm, Reduce ROIs**. Fourth, the MLC leaf positions are always available from the EPID images, which can serve as a useful landmark for fiducial position estimation because the fiducials should be either detected or in the MLC leaf blocked area. Finally, the 3D movement of the markers captured by the pretreatment 4D CBCT and simulation 4D CT is also available for positional prediction. For example, an elliptic ROI may be used for a known tumor- motion direction instead of a circular ROI. This will reduce the size of possible MV projection locations in certain directions. Furthermore, it would reduce the length of 1D possible

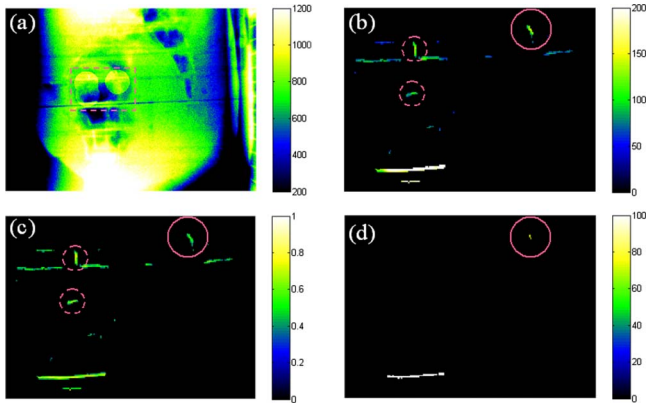

FIG. 5. Typical fiducial tracking. (a) Projection image in which the ROIs were highlighted. (b) Intensity results of pattern matching in the dash rectangle region of (a). (c) R^2 results of pattern matching in the dash rectangle region of (a). (d) Qualified features after the primary search.

MV projection locations predicted by orthogonal kV imaging results.

III. RESULTS

- **An Example of fiducial tracking**

  Figure 5 illustrates a difficult fiducial tracking case on a lateral MV image. The ROIs for three fiducials were predicted by the planning CT results and highlighted in Fig. 5(a), in which the dash rectangle displayed a region including all ROIs. After pattern matching was performed on every pixel in the ROIs, intensity and R^2 results were obtained as shown in Figs. 5(b) and 5(c), respectively. The intensity and R^2 thresholds were determined based on the maximum values of that ROI group and predefined minimum values. After threshold screening, only one feature was qualified as a fiducial [enclosed by a solid circle in Fig. 5(d)] while another feature was rejected because its length was too long.

  The second search then followed. The positions of undetected markers were closely estimated by the relative shifts among markers as enclosed by the small dashed circles in Figs. 5(b) and 5(c). After the thresholds were set at lower values, all markers were successfully detected.

- **Speed limit for detecting moving fiducials**

  MV and kV image series were analyzed with the motion platform moving at different periods. Figure 6(a) illustrates the projection locations of one marker when the motion platform was moving at an amplitude of 10.0 mm with a period of 4 s. The traces were fit to sine waves shown in the Fig. 6(a). The fitting results indicated that the motion amplitudes for both axes were 3.38 and 9.49 mm, respectively. This means the total amplitude is 10.07 mm ($=\sqrt{3.38^2+9.49^2}$), which is very close to the nominal amplitude (10.0 mm). Figure 6(b) illustrates the difference between measured projections and fitting results and the variations are less than 0.8 mm.

  Images of the moving phantom were analyzed to test

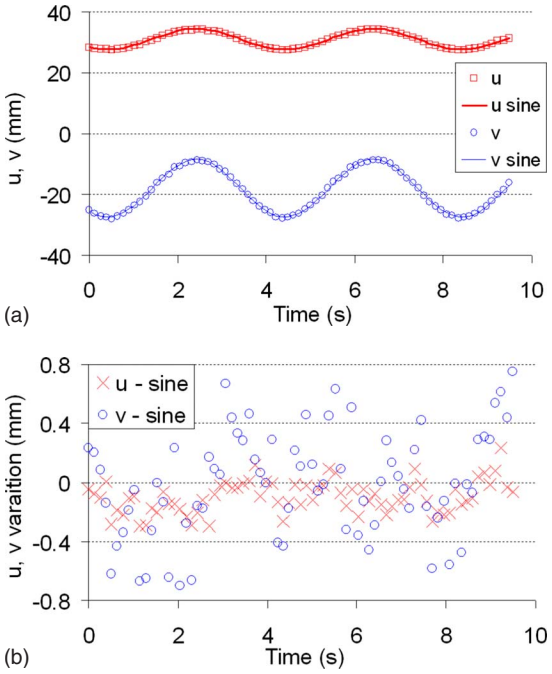

FIG. 6. Marker Detecting Accuracy. (a) Measured the projections against fitting results. (b) Differences between measured the projections against fitting results.

the detection efficiency for moving fiducials. In total, 877 kV and 456 MV images on both lateral (90° gantry angle) and AP directions were acquired and analyzed for the motion study. It is always easier to detect markers on the AP images than on the LAT images, partially because of the increased scattering at the LAT direction. All markers in kV images and AP MV images (either 6 MV or 15 MV energy) were successfully detected (detection efficiency of 100%). For the difficult cases, detection efficiencies on LAT MV images are illustrated in Fig. 7. A detection efficiency of better than 95% is achieved for both MV energies when the motion period is 4 s or longer, which correlates to a maximum linear speed of 1.6 cm/s or slower.

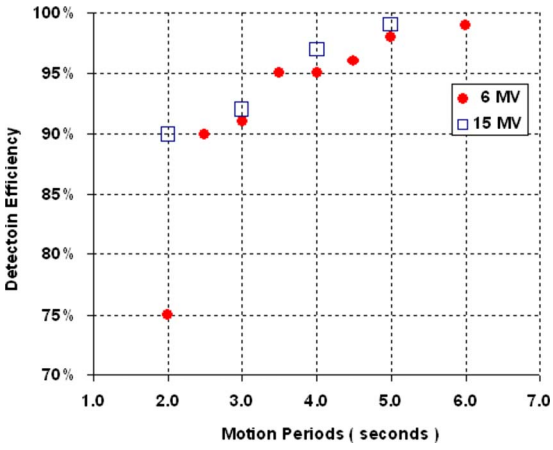

FIG. 7. Detection efficiencies of moving markers on LAT MV images of dual energies.

TABLE I. Summary of the kV detection efficiencies affected by MV field size and kV SID. Two efficiencies present MV field at AP and LAT directions, respectively.

kV SID (cm)		181.8		166.7		150.0	
MV direction		AP	LAT	AP	LAT	AP	LAT
MV field size (cm^2)	10×10	100%	100%	100%	100%	100%	100%
	15×15	100%	100%	100%	100%	100%	4%
	26×20	100%	76%	61%	13%	6%	1%

- **Effects of MV beam scattering on kV imaging**

  Usually scattering of the simultaneous MV and kV beams can cause concern for degrading the quality of the kV image. Fortunately, here only the fiducial markers are of interest and our analysis is capable of suffering a certain degree of scattering. The kV SID was extended further to reduce the scattering from MV beams; 842 kV images were acquired and analyzed while varying the SID and MV field size; the detection efficiency results are summarized in Table I. As expected, either a smaller MV field or a larger SID leads to better detection. It was found that the markers in kV images could be successfully analyzed even with the scattering from a common treatment MV field (10×10 cm or less). In addition, when our 3DCRT and IMRT plans were delivered, more than 5000 kV images were acquired and analyzed and all markers were successfully detected with a detection efficiency of 100%. This guarantees that kV imaging is always applicable for tracking fiducials during treatment.
- **Tracking FMs in the presence of a MLC**

  The IMRT plan was delivered once without phantom motion and once with a motion period of 4.0 s. All MV and kV images were acquired and analyzed. Special attention was paid on treatment segments with fiducials partially or completely blocked by the MLC. Figure 8 illustrates fiducial tracking on the MV field at a gantry angle of 235° with the static phantom. The fiducial coordinates obtained from orthogonal kV images were used to help locate projections on MV images [as shown in Fig. 8(a)]. The possible MV projection might not be exactly horizontal due to the divergence of the kV x-ray trace (as discussed in the Appendix). As long as a fiducial was detected at any segment [Figs. 8(c)–8(i)], the blocked fiducials could be estimated very closely by fiducial relative positions (circles in the MLC blocked area) and common axis kV coordinates (solid lines). The estimated position was limited on a horizontal line with a length corresponding internal deformation up to ±5 mm. It is still possible that all fiducials are outside of the MV field because of small IMRT segments as shown in Fig. 8(b). In this case, the possible positions could be estimated as elliptic ROIs by 3D planning CT data and available 4D CT results. Their long and short axes correspond to possible motion of ±2 cm and ±1 cm in two directions, respectively. The orthogonal kV imaging results limit the estimation to horizontal lines with a length corresponding motion up to ±1 cm.

  The 3DCRT plan was delivered three times with the motion period varied at 2.0, 3.0, and 4.0 s. All MV and kV images were acquired and analyzed. Figure 9 displays the simultaneous MV and kV images when the phantom was moving. Most of the markers were suc-

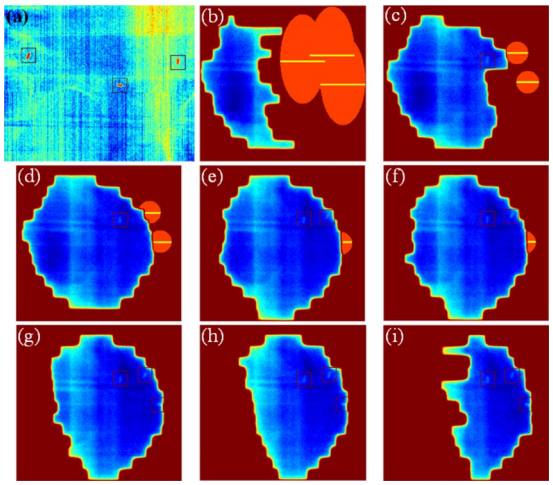

FIG. 8. Detect fiducials during an IMRT treatment. (a) Orthogonal kV image. (b)–(i) MV images for every segment. Detected fiducials were enclosed in square boxes. Ovals or circles in the MLC blocked region indicate the predicted fiducial projections and the horizontal line indicate the predicted fiducial projections based on orthogonal kV imaging results.

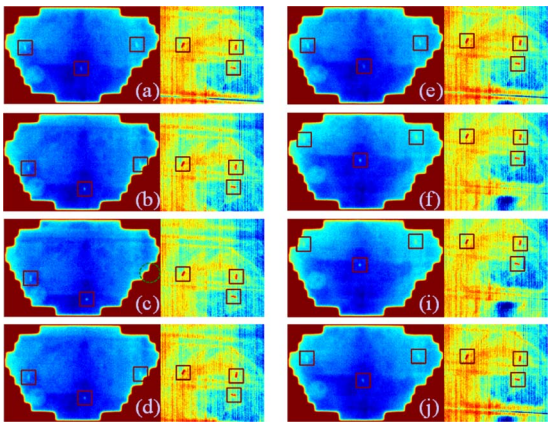

FIG. 9. Simultaneous MV and kV images with a MV gantry angle of 180° and a motion period of 4 s.

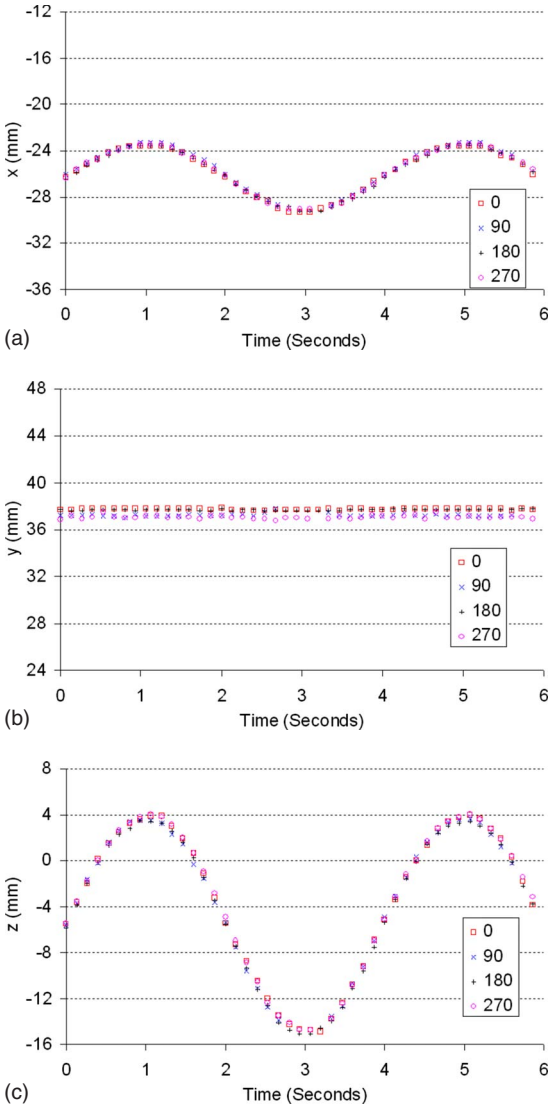

FIG. 10. Three-dimensional coordinates of one marker during the treatment. Results from four fields were synchronized for comparison purpose; (a) x coordinates, (b) y coordinates, (c) z coordinates.

cessfully detected as enclosed in solid rectangles. Nearly real-time 3D positions of fiducial markers were calculated at all fields based on Eqs. (7)–(11). After synchronizing the results from different fields, it was found that results from different fields were within ± 0.8 mm of their average positions. Figure 10 illustrates 3D coordinates of one moving marker in every field with a period of 4 s.

It should be noted that the presence of a MLC does not affect the detection efficiency dependence on motion speed and all fiducial markers on every kV image were successfully detected.

- **Performance of analysis software**

Special attention was paid on the analysis software programming. It is essential to compute the location of a marker quickly so to be able to track the markers at a speed of 10 fps or higher. Most of the calculation time was spent on the pattern matching, including determining orientation and calculating intensity and R^2. A complete search on 1024×768 pixels image costs about 1 s. The searching region of three markers with a radius of 75 pixels reduces the calculation time by an order of magnitude. The average search time for three markers was 0.08 s per frame.

Basically, kV and MV images could be analyzed independently. It is generally much easier to track markers on kV images than on MV images not only because kV images have better contrast but also because fiducials are always visible in kV images. However, this does not mean that double the calculation time is needed for simultaneous kV and MV image analysis because the kV tracking results might be used to reduce MV ROIs as shown in Fig. 4 in addition to the other two methods to reduce ROIs. This process significantly reduces the size of ROIs on MV images and further reduces the computation time. It is found that 0.1 s analysis time per kV/MV pair is achievable on our current single CPU architecture. Reduced computation time is expected if parallel computation is implemented on a multiple-core processor.

IV. DISCUSSION

The four studies presented in this article pave the way to track 3D positions of multiple moving fiducial markers during treatment in nearly real time. We demonstrate that our algorithm is capable of tracking fast moving fiducial markers by simultaneous kV and treatment MV imaging. Furthermore, the analysis speed is fast enough to report nearly real-time 3D positions of the markers. It is also worthwhile to mention that this procedure does not need any assumed motion model. Although all motion experiments were performed on a periodic moving platform, the algorithm does not take this periodicity into consideration, meaning these results should just as easily apply to nonperiodic motion. This is also why the term nearly real-time 3D position was used instead of 4D position because the terminology of 4D usually refers to a periodic motion particularly when it is associated with 4D CT. This procedure detects any regular, irregular, or sudden motion as long as the maximum speed is not very fast.

We can track marker motion up to a period of 2 s in kV images, not only because of much higher contrast of kV images than MV images, but also because of its higher capture speed (15 fps). Currently, the acquisition speed of the MV imaging is less than 8 fps, which means that the marker may move about 2 mm ($\sim$7.5 pixels on imager) at a speed of 1.6 cm/s during one acquisition (marker width $\sim$5 pixels). The blurring induced by motion and small size of the marker make it difficult to track fiducials on MV images, particularly those with low image quality. It should also be noted that better hardware will improve performance, e.g., quicker MV image acquisition.

This method is suitable for tracking any tumor motion as long as fiducial markers or surgical clips are available. It is not limited to a certain type of site although the studies were performed on a pelvic phantom.

The proposed procedure will be an economic solution to nearly real-time tracking of tumor motion since more and more linear accelerators are coming equipped with an onboard kV imaging system. This procedure does not need any extra expensive equipment such as multiple kV imaging sets.

Another advantage of this procedure over stereoscopic kV tracking systems is that using the treatment beam as part of tracking reduces extra dose to the patient. Although kV imaging dose is still a concern, we would like to emphasize that the patient dose from a single kV imaging set here is 50% less than that from stereoscopic kV imaging sets. In this study, we used the typical kV CBCT imaging parameters (125 kV, 80 ms, and 25 mA). It has been reported that the dose to the soft tissue for such a CBCT scan (with 630 images) is ~5 cGy.[33] Since an acquisition speed of 7.5 fps is sufficient, the kV dose is about 3.6 cGy/Min (5 cGy/630*(7.5/s)=0.06 cGy/s). A typical IMRT treatment has a beam on time of about 2 min for a 200 cGy dose delivery to the target. This implies that the kV imaging dose is about 7.2 cGy. However, this represents the worst case scenario where the kV beam is on throughout the IMRT beam delivery process. In reality, it is not necessary to keep the kV imaging system on all the time. The kV imaging may be switched off during the step mode of IMRT delivery. In addition, the kV field size can be reduced according to the fiducial motion range. All these strategies may further reduce the kV imaging dose.

The proposed hybrid MV/kV imaging technique is readily applicable to facilitate conventional 3D radiation therapy by providing real-time information of the implanted fiducials. When using IMRT MV beam for in-line imaging, a potential difficulty is that the fiducials may be partially or completely blocked by the MLC leaves at a certain segment(s). There are four sources of information that help to estimate the 3D coordinates of the MLC-blocked fiducial in this situation. First, the coordinates of the fiducial in the plane perpendicular to the kV beam are still available from kV imaging. This piece of information is very valuable because it significantly reduces the dimensionality of the problem. Second, the fiducial kinetics attained by the kV/MV system at earlier time when the marker(s) are not blocked can be utilized to adaptively predict the "missing" coordinate of the marker in combination with the kV information. Third, the MLC leaf positions are always available from the EPID images, which can serve as a useful landmark for fiducial position estimation. Finally, the 3D movement of the markers captured by the pretreatment CBCT and planning CT is also available as *a priori* knowledge for better positional estimation. The development of such a multiple input single output adaptive prediction algorithm is still in progress. Because there is only one coordinate that needs to be estimated for a short interval of time, we foresee no major difficulty in accomplishing an accurate positional estimation. This remains true in a rare situation when all the fiducials are blocked by a MLC segment. For certain types of tumors that deform little during the treatment process (e.g., the prostate), the positions of unblocked fiducials can be employed as landmarks in allocating the MLC-blocked fiducial(s).

During our 3DCRT verification plan delivery, at least two of three fiducials were visible in every field even when the phantom was on a motion platform. All fiducials were visible in 95% of the segments. During the delivery of the verification IMRT plan, at least one fiducial was visible in about 75% of the segments. This percentage is highly dependent on the case and the treatment planning system. To increase the visible time of a fiducial, it is possible to add one or more imaging segments (i.e., a segmented field with small monitor unit for the purpose of imaging the fiducials) to the treatment IMRT leaf sequences to facilitate the detection of a fiducial at a certain point of IMRT delivery. Another avenue of research is to take the fiducial information into consideration during the IMRT inverse planning process. With the development of segment-based dose optimization methods,[34,35] it should be feasible to ensure the visibility of at least one fiducial during the inverse planning process. Of course, the addition of this type of constraint in inverse planning may compromise the achievable dose distribution. But it is arguable that the trade-off will likely be minimal because, after all, the fiducials are all inside the tumor target volume and represent high dose points. We are currently actively studying this issue and the results will be reported elsewhere.

V. CONCLUSION

The four studies presented in this article pave the way to track nearly real-time 3D positions of multiple moving fiducial markers during treatment. It is demonstrated that this proposed process is capable of tracking fast moving fiducial markers (up to 1.6 cm/s) by analyzing simultaneous kV and treatment MV images. The analysis speed is as fast as 10 fps and can report nearly real-time 3D positions of markers with submillimeter accuracy.

ACKNOWLEDGMENTS

This work was supported in part by grants from the Department of Defense (PC040282), the National Cancer Institute (1R01 CA104205), and the Komen Breast Cancer Foundation (BCTR0504071).

APPENDIX

Any fiducial projects on kV imager at P, (u_{kV}, v_{kV}). This fiducial must be on the line of KP (as shown in Fig. 11):

$$\begin{cases} x = R_{kV} - \gamma \cdot F_{kV} \\ y = \gamma \cdot u_{kV} \\ z = \gamma \cdot v_{kV} \end{cases} \quad \text{(A1)}$$

While γ is arbitrary, F_{kV} and R_{kV} are the source-imager distance (SID) and the source-axis distance (SAD) of kV system, respectively.

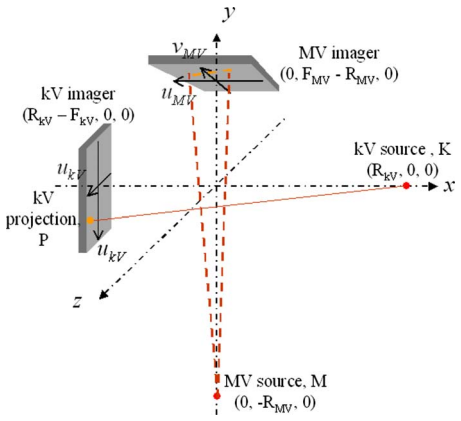

FIG. 11. Schematic diagram of relationship between kV and MV projections of the same fiducial.

This fiducial projects on MV imager on plane MKP (as shown in Fig. 11),

$$x + b \cdot (y + R_{\mathrm{MV}}) + c \cdot z = 0, \tag{A2}$$

while b and c are constants and R_{MV} is the SAD of MV system. Input Eq. (A1) to Eq. (A2), we have

$$(R_{\mathrm{kV}} - \gamma \cdot F_{\mathrm{kV}}) + b \cdot \gamma \cdot u_{\mathrm{kV}} + b \cdot R_{\mathrm{MV}} + c \cdot \gamma \cdot v_{\mathrm{kV}} = 0$$

or

$$R_{\mathrm{kV}} + b \cdot R_{\mathrm{MV}} + \gamma \cdot (-F_{\mathrm{kV}} + b \cdot u_{\mathrm{kV}} + c \cdot v_{\mathrm{kV}}) = 0. \tag{A3}$$

Since γ is arbitrary, we get

$$b = -\frac{R_{\mathrm{kV}}}{R_{\mathrm{MV}}} \tag{A4}$$

and

$$-F_{\mathrm{kV}} + b \cdot u_{\mathrm{kV}} + c \cdot v_{\mathrm{kV}} = 0,$$

or

$$c = \frac{F_{\mathrm{kV}} R_{\mathrm{MV}} + R_{\mathrm{kV}} u_{\mathrm{kV}}}{R_{\mathrm{MV}} v_{\mathrm{kV}}}. \tag{A5}$$

The projection on MV imager [B, $(u_{\mathrm{MV}}, v_{\mathrm{MV}})$] lies on a line in the MV imager plane $v = F_{\mathrm{MV}}$-R_{MV}, so that the projection locations of A and B have a relationship:

$$\frac{v_{\mathrm{MV}}}{v_{\mathrm{kV}}} = \frac{F_{\mathrm{MV}} R_{\mathrm{kV}} + R_{\mathrm{MV}} u_{\mathrm{MV}}}{F_{\mathrm{kV}} R_{\mathrm{MV}} + R_{\mathrm{kV}} u_{\mathrm{kV}}}$$

or

$$(F_{\mathrm{kV}} R_{\mathrm{MV}} + R_{\mathrm{kV}} u_{\mathrm{kV}}) \cdot v_{\mathrm{MV}} - R_{\mathrm{MV}} v_{\mathrm{kV}} u_{\mathrm{MV}} = F_{\mathrm{MV}} R_{\mathrm{kV}} v_{\mathrm{kV}}. \tag{A6}$$

Typically, both MV and kV systems have a SAD of 100 cm and a SID of 150 cm, approximately,

$$\frac{v_{\mathrm{MV}}}{v_{\mathrm{kV}}} \approx 1 + \frac{u_{\mathrm{kV}} - u_{\mathrm{MV}}}{F_{\mathrm{MV}}}.$$

For a small target, whose fiducials are within a region with a radius of 2 cm, $|v_{\mathrm{MV}}/v_{\mathrm{kV}}|$ is usually very close to unity within ±4%, i.e., v_{MV} and v_{kV} are close to each other.

[a]Author to whom correspondence should be addressed. Electronic mail: lei@reyes.stanford.edu

[1]IMRT Collaborative Working Group, "Intensity-modulated radiotherapy: Current status and issues of interest," Int. J. Radiat. Oncol., Biol., Phys. **51**(4), 880–914 (2001).
[2]J. M. Galvin *et al.*, "Implementing IMRT in clinical practice. A joint document of the American Society for Therapeutic Radiology and Oncology and the American Association of Physicists in Medicine," Int. J. Radiat. Oncol., Biol., Phys. **58**(5), 1616–1634 (2004).
[3]K. Kitamura *et al.*, "Three-dimensional intrafractional movement of prostate measured during real-time tumor-tracking radiotherapy in supine and prone treatment positions," Int. J. Radiat. Oncol., Biol., Phys. **53**(5), 1117–1123 (2002).
[4]J. M. Crook *et al.*, "Prostate motion during standard radiotherapy as assessed by fiducial markers," Radiother. Oncol. **37**(1), 35–42 (1995).
[5]R. I. Berbeco *et al.*, "Residual motion of lung tumors in end-of-inhale respiratory gated radiotherapy based on external surrogates," Med. Phys. **33**(11), 4149–4156 (2006).
[6]Y. Seppenwoolde *et al.*, "Precise and real-time measurement of 3D tumor motion in lung due to breathing and heartbeat, measured during radiotherapy," Int. J. Radiat. Oncol., Biol., Phys. **53**(4), 822–834 (2002).
[7]Y. Xie *et al.*, "Intrafraction motion of the prostate in cyberknife hypofractionated radiotherapy," Int. J. Radiat. Oncol., Biol., Phys. (2007). (submitted).
[8]K. L. Zhao *et al.*, "Evaluation of respiratory-induced target motion for esophageal tumors at the gastroesophageal junction," Radiother. Oncol. **84**(3), 283–289 (2007).
[9]H. Shirato *et al.*, "Speed and amplitude of lung tumor motion precisely detected in four-dimensional setup and in real-time tumor-tracking radiotherapy," Int. J. Radiat. Oncol., Biol., Phys. **64**(4), 1229–1236 (2006).
[10]L. Xing *et al.*, "Overview of image-guided radiation therapy," Med. Dosim. **31**(2), 91–112 (2006).
[11]M. J. Murphy, "Fracking moving organs in real time," Semin. Radiat. Oncol. **14**(1), 91–100 (2004).
[12]P. C. Chi *et al.*, "Relation of external surface to internal tumor motion studied with cine CT," Med. Phys. **33**(9), 3116–3123 (2006).
[13]H. Shirato *et al.*, "Real-time tumour-tracking radiotherapy," Lancet **353**(9161), 1331–1332 (1999).
[14]P. Kupelian *et al.*, "Multi-institutional clinical experience with the Calypso System in localization and continuous, real-time monitoring of the prostate gland during external radiotherapy," Int. J. Radiat. Oncol., Biol., Phys. **67**(4), 1088–1098 (2007).
[15]A. L. Boyer *et al.*, "A review of electronic portal imaging devices (EPIDs)," Med. Phys. **19**(1), 1–16 (1992).
[16]L. Dong *et al.*, "Verification of radiosurgery target point alignment with an electronic portal imaging device (EPID)," Med. Phys. **24**(2), 263–267 (1997).
[17]M. G. Herman *et al.*, "Technical aspects of daily online positioning of the prostate for three-dimensional conformal radiotherapy using an electronic portal imaging device," Int. J. Radiat. Oncol., Biol., Phys. **57**(4), 1131–1140 (2003).
[18]P. J. Keall *et al.*, "On the use of EPID-based implanted marker tracking for 4D radiotherapy," Med. Phys. **31**(12), 3492–3499 (2004).
[19]H. Dehnad *et al.*, "Clinical feasibility study for the use of implanted gold seeds in the prostate as reliable positioning markers during megavoltage irradiation," Radiother. Oncol. **67**(3), 295–302 (2003).
[20]A. Nederveen, J. Lagendijk, and P. Hofman, "Detection of fiducial gold markers for automatic on-line megavoltage position verification using a marker extraction kernel (MEK)," Int. J. Radiat. Oncol., Biol., Phys. **47**(5), 1435–1442 (2000).
[21]A. J. Nederveen, J. J. Lagendijk, and P. Hofman, "Feasibility of automatic marker detection with an a-Si flat-panel imager," Phys. Med. Biol. **46**(4), 1219–1230 (2001).
[22]J. Pouliot *et al.*, "(Non)-migration of radiopaque markers used for on-line localization of the prostate with an electronic portal imaging device," Int. J. Radiat. Oncol., Biol., Phys. **56**(3), 862–866 (2003).
[23]D. C. Schiffner *et al.*, "Daily electronic portal imaging of implanted gold seed fiducials in patients undergoing radiotherapy after radical prostatectomy," Int. J. Radiat. Oncol., Biol., Phys. **67**(2), 610–619 (2007).

[24]L. Smith *et al.*, "Automatic detection of fiducial markers in fluoroscopy images for on-line calibration," Med. Phys. **32**(6), 1521–1523 (2005).
[25]H. Shirato *et al.*, "Physical aspects of a real-time tumor-tracking system for gated radiotherapy," Int. J. Radiat. Oncol., Biol., Phys. **48**(4), 1187–1195 (2000).
[26]T. R. Willoughby *et al.*, "Evaluation of an infrared camera and X-ray system using implanted fiducials in patients with lung tumors for gated radiation therapy," Int. J. Radiat. Oncol., Biol., Phys. **66**(2), 568–575 (2006).
[27]X. Tang, G. C. Sharp, and S. B. Jiang, "Fluoroscopic tracking of multiple implanted fiducial markers using multiple object tracking," Phys. Med. Biol. **52**(14), 4081–4098 (2007).
[28]K. Kitamura *et al.*, "Tumor location, cirrhosis, and surgical history contribute to tumor movement in the liver, as measured during stereotactic irradiation using a real-time tumor-tracking radiotherapy system," Int. J. Radiat. Oncol., Biol., Phys. **56**(1), 221–228 (2003).
[29]R. D. Wiersma, W. Mao, and L. Xing, "Combined kV and MV imaging for real-time tracking of implanted fiducial markers," Med. Phys. **35**(4), 1191–1198 (2008).
[30]W. Mao, R. Wiersma, and L. Xing, "Fast internal marker tracking algorithm for onboard MV and kV imaging systems," Med. Phys. **35**(5), 1942–1949 (2008).
[31]W. Luo *et al.*, "Effect of Mv scatter on Kv image quality during simultaneous Kvmv imaging," Int. J. Radiat. Oncol., Biol., Phys. **69**(3), S671 (2007).
[32]W. Mao *et al.*, "CT image registration in sinogram space," Med. Phys. **34**(9), 3596–3602 (2007).
[33]N. Wen *et al.*, "Dose-delivered from Varian's CBCT to patients receiving IMRT for prostate cancer," Phys. Med. Biol. **52**(8), 2267–2276 (2007).
[34]D. M. Shepard *et al.*, "Direct aperture optimization: A turnkey solution for step- and-shoot IMRT," Med. Phys. **29**(6), 1007–1018 (2002).
[35]C. Cotrutz and L. Xing, "Segment-based dose optimization using a genetic algorithm," Phys. Med. Biol. **48**(18), 2987–2998 (2003).